

This is the author's peer reviewed, accepted manuscript. However, the online version of record will be different from this version once it has been copyedited and typeset.

PLEASE CITE THIS ARTICLE AS DOI: 10.1063/5.0048604

## Terahertz Faraday rotation of aluminum-substituted barium hexaferrite

A.N. Grebenchukov,<sup>1, a)</sup> V.I. Ivanova,<sup>2</sup> G.I. Kropotov,<sup>1</sup> and M.K. Khodzitsky<sup>1</sup>

<sup>1)</sup>TYDEX LLC, St.Petersburg, 194292, Russia

<sup>2)</sup>Ferrite-Domen Scientific Research Institute, St. Petersburg, 196084, Russia

(Dated: 28 April 2021)

Faraday rotation effect of magnetized hexagonal ferrites  $\text{BaAl}_x\text{Fe}_{12-x}\text{O}_{19}$  ( $x = 1.4, 2.0$ ) with varied density in the frequency range of 0.1–1.0 THz was investigated using terahertz (THz) time-domain spectroscopy. Broadband polarization rotation up to  $20^\circ$  for 1-mm thick hexaferrite was demonstrated at room temperature. It was shown that the value of Faraday rotation can be effectively controlled by varying hexaferrite sample density as well as Al concentration. From the experimental data, full permittivity tensor characterization of different hexaferrite samples was extracted to double-check the calculation of Faraday rotation. The obtained results demonstrate prospects for utilization of  $\text{BaAl}_{1.4}\text{Fe}_{10.6}\text{O}_{19}$  hexaferrite with the highest density as a broadband self-biased complete THz isolator with moderate insertion losses below  $5 \text{ cm}^{-1}$  in the range up to 0.4 THz.

Electromagnetic non-reciprocity is a key feature of one-way propagating devices. Their realization at terahertz (THz) frequencies is an important challenge. Since THz isolation is crucial for eliminating back-reflected radiation resulting in source protection and noise-canceling<sup>1</sup>. Well known way for achieving non-reciprocity is in the utilization of magneto-optical effects<sup>2</sup>. For instance, the isolation based on the Faraday effect requires configuration with two additional linear polarizers oriented in  $45^\circ$  relative to each other. However, still, there is a lack of high-performance non-dispersive THz magneto-optical materials. Several materials have been proposed as a suitable magneto-optical medium, including graphene<sup>3,4</sup>, high-mobility narrow-gap semiconductor<sup>5-7</sup>, TSAG crystals<sup>8</sup>, La: YIG crystals<sup>9</sup>, and ferrite materials<sup>10,11</sup>. However, in most cases, to achieve Faraday rotation external magnetic field should be applied. Alternatively, magnetic-free approaches to achieve non-reciprocity have recently been proposed. Among them, spatiotemporally modulated media<sup>12</sup> and nonlinear materials<sup>13</sup> can be distinguished. However, for the most part, the practical realization of such alternative systems is too complicated.

Promising candidates for utilization as a basis of THz nonreciprocal devices are M-type hexaferrite ( $\text{MFe}_{12}\text{O}_{19}$ )<sup>14</sup>. This type of hexaferrite possesses strong non-dispersive gyrotropic features even in the THz range due to the high anisotropy field<sup>15</sup>. Also, hexaferrite can be fabricated with permanent magnet features due to high magnetocrystalline anisotropy, i.e., the magnetization state is maintained without applying an external magnetic field. This fact resulting in magneto-optical device miniaturization<sup>16</sup>. Although the hexaferrite samples allow self-biased wideband nonreciprocal polarization rotation, the insertion losses of the most magnet material are sufficiently large<sup>10</sup>. Within this context, searching for ferromagnetic materials with a high gyrotropic response and low absorption in the THz frequency range is of great importance. In this paper, we investigated the Faraday rotation effect in magnetized Al substituted Ba hexaferrite ( $\text{BaAl}_x\text{Fe}_{12-x}\text{O}_{19}$ ) of varying density with two different dopant concentration  $x(\text{Al})$  of 1.4 and 2.0 in the range between 0.1 and 1 THz.

<sup>a)</sup>Electronic mail: grebenchukov\_a@mail.ru

TABLE I. The  $\text{BaAl}_x\text{Fe}_{12-x}\text{O}_{19}$  samples.

Sample	Al concn.	Compound	$\rho$ (g/cm <sup>3</sup> )	$M$ (kA/m)
1	$x = 1.4$	$\text{BaAl}_{1.4}\text{Fe}_{10.6}\text{O}_{19}$	4.01	164
2	$x = 1.4$	$\text{BaAl}_{1.4}\text{Fe}_{10.6}\text{O}_{19}$	4.50	187
3	$x = 1.4$	$\text{BaAl}_{1.4}\text{Fe}_{10.6}\text{O}_{19}$	4.97	207
4	$x = 2.0$	$\text{BaAl}_{2.0}\text{Fe}_{10}\text{O}_{19}$	4.07	114
5	$x = 2.0$	$\text{BaAl}_{2.0}\text{Fe}_{10}\text{O}_{19}$	4.57	142
6	$x = 2.0$	$\text{BaAl}_{2.0}\text{Fe}_{10}\text{O}_{19}$	4.95	169

The experimental results show broadband Faraday rotation up to  $20^\circ$  with moderate insertion losses in the range below 0.4 THz. Also, the tunability of non-reciprocal polarization rotation value by varying sample density or Al dopant concentration was demonstrated.

The  $\text{BaAl}_x\text{Fe}_{12-x}\text{O}_{19}$  samples were synthesized from  $\text{Fe}_2\text{O}_3$  and  $\text{Al}_2\text{O}_3$  oxides and  $\text{BaCO}_3$  carbonate in stoichiometric proportions. The initial components were mixed and annealed in air at  $1220\text{--}1280^\circ\text{C}$  for 4–6 hours. The resulting ferrite powder was subjected to wet grinding in ethanol for 20–24 hours. Then the samples were pressed in a constant magnetic field at a specific pressing of 300–500 kg/cm<sup>2</sup>. After drying, the samples were annealed at a temperature of  $1250\text{--}1350^\circ\text{C}$  in an oxygen atmosphere and polished to the desired size. The list of obtained hexaferrite samples is presented in Table I. Al concentration was controlled by atomic absorption spectrometry using hexaferrite solution in hydrochloric acid. As the hexaferrite is a porous material, the apparent relative density of samples was measured using a pycnometer.

In this work, the magneto-optical properties of hexaferrite samples were investigated by the commercial THz time-domain spectroscopy (THz-TDS) system (Menlo Systems TERA K8). The Faraday rotation spectra measurement scheme is shown in Fig. 1. The hexaferrite sample was placed between two fixed polarizers with an orientation set to  $0^\circ$ . The first and the last ones were defining the vertical linear polarization state for generated and detected signals. A rotatable THz polarizer was set at  $+45^\circ$  and  $-45^\circ$  to get information about the polarization state of THz radiation transmitted through the gyrotropic hexaferrite<sup>17</sup>.

The Faraday rotation angle can be calculated using the following relation<sup>18</sup>:

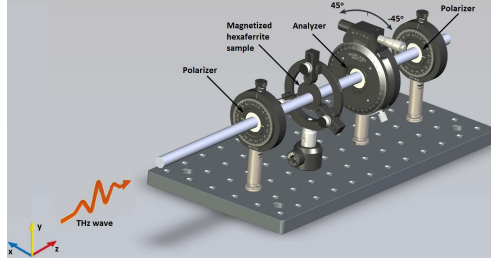


FIG. 1. The experimental THz polarimetry setup.

$$\theta_F = 0.5 \arctan \frac{2\Re(E_x^* E_y)}{|E_x|^2 - |E_y|^2}. \quad (1)$$

Two mutually orthogonal complex  $E$  components of radiation transmitted through the sample can be defined using the complex electric field components of radiation transmitted through the whole system shown in Fig 1 when the rotatable polarizer was set at  $+45^\circ$  and  $-45^\circ$  position (complex  $E_{+45}$  and  $E_{-45}$ , correspondingly). In this case, the relation between  $E$  components takes the following form<sup>19</sup>:

$$\begin{aligned} E_x &= E_{+45} + E_{-45} \\ E_y &= -E_{+45} + E_{-45}. \end{aligned} \quad (2)$$

The transmission spectra were measured for non-magnetized hexaferrite samples using the setup as in Fig. 1 with all polarizers oriented at  $0^\circ$ . Corresponding amplitude transmission spectra of six 1-mm thick hexaferrite samples are shown in Fig. 2a. Obtained spectra show a linear decrease of THz transmission with increasing of the ferrite density in the range below 0.4 THz. While for higher frequencies the amount of Al has a stronger effect on transmission features, i.e., in that frequency range samples with  $x = 2.0$  transmit more than samples with  $x = 1.4$  regardless of sample density. Corresponding absorption spectra for each non-magnetized hexaferrite sample were calculated as follows in Fig. 2b. Detailed calculation method from standard THz-TDS spectroscopy measurement was well described previously<sup>20</sup>.

The absorption spectra correlate with frequency dependencies of the transmission coefficient. As seen from Fig. 2b the absorption coefficient below 0.4 THz is less than  $5 \text{ cm}^{-1}$  for every investigated sample. Despite the strong increase in absorption at higher frequencies, the increase in the concentration of diamagnetic Al ions from  $x = 1.4$  to  $x = 2.0$  leads to loss decreasing in that range.

Then, the samples were permanently magnetized up to the saturation magnetization. Corresponding magnetization ( $M$ ) values are presented in Table I. Faraday rotation spectra obtained experimentally for six hexaferrite samples at the magnetization saturation are shown as lines in Fig. 3.

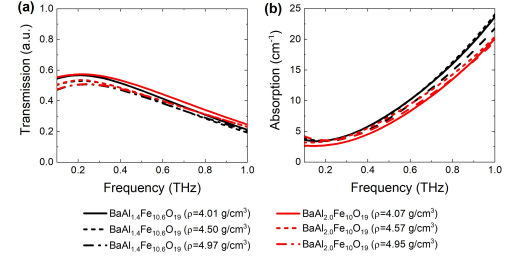


FIG. 2. The transmission (a) and absorption (b) spectra of 1-mm thick Al substituted Ba hexaferrite samples with different material densities and Al substitution amounts.

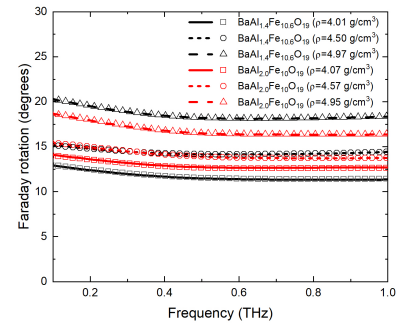


FIG. 3. Faraday rotation spectra of 1-mm thick Al substituted Ba hexaferrite samples with different material densities and Al substitution amounts. Lines represent data obtained using Eq. 1, symbols represent data obtained using Eq. 10.

In the considered frequency band, the Faraday rotation spectra of each ferrite sample exhibit a low-dispersive character. The maximum Faraday rotation value of  $20^\circ$  in 1-mm thick  $\text{BaAl}_{1.4}\text{Fe}_{10.6}\text{O}_{19}$  with  $\rho = 4.97 \text{ g/cm}^2$  is achieved. The rotation effect strongly depends on sample density. High-density ferrites enable achieving higher rotation angle values. However, the sensitivity of the polarization rotatory power to the sample density decreases as the Al dopant concentration increases from  $x = 1.4$  to  $x = 2.0$ . That can be associated with the decrease in the saturation magnetization for higher diamagnetic Al ions concentrations<sup>21</sup>. The propagation reversal of the THz wave leads to reversal of the polarization rotation sign, confirming non-reciprocal features of the hexaferrite samples. Thus, the most perspective hexaferrite sample to induce the required  $45^\circ$  rotation for full isolation is a high-density  $\text{BaAl}_{1.4}\text{Fe}_{10.6}\text{O}_{19}$  sample with proportionally increased thickness.

To obtain a parameter that describes the Faraday rotation taking into account insertion losses, the figure of merit (FOM)

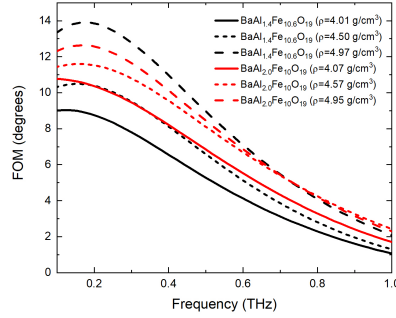


FIG. 4. The figure of merit spectra of 1-mm thick Al substituted Ba hexaferrite samples with different material densities and Al substitution amounts.

was introduced as:

$$\text{FOM} = \theta_F \exp(-\alpha d), \quad (3)$$

where  $\alpha$  is the absorption (Fig 2b) and  $d = 1$  mm is the sample thickness. Corresponding FOM spectra for hexaferrite samples are presented in Fig. 4.

As it is seen from the FOM spectra (Fig. 4), the best FOM corresponds to  $\text{BaFe}_{10.6}\text{Al}_{1.4}\text{O}_{19}$  with  $\rho = 4.97$   $\text{g}/\text{cm}^3$  in the spectral band up to 0.6 THz.

Let us consider the electromagnetic wave propagation along the  $z$ -axis through a normally magnetized hexaferrite disk. Since the ferromagnetic resonance in hexaferrite ceramics is at frequencies well below the THz range, the magnetic losses are negligible in comparison with dielectric ones<sup>22</sup>. In that case, the relative dielectric tensor expressed as<sup>2,19</sup>:

$$\boldsymbol{\varepsilon}(\omega) = \begin{pmatrix} \varepsilon_s(\omega) & j\varepsilon_a(\omega) & 0 \\ -j\varepsilon_a(\omega) & \varepsilon_s(\omega) & 0 \\ 0 & 0 & \varepsilon_z(\omega) \end{pmatrix}. \quad (4)$$

Here, off-diagonal elements of the tensor determine the magneto-optical response of the hexaferrite samples. The diagonal  $\varepsilon_{xx}(\omega) = \varepsilon_s(\omega)$  and off-diagonal  $\varepsilon_{xy}(\omega) = i\varepsilon_a(\omega)$  complex components of permittivity tensor are expressed through refractive indices for right and left circular polarization as

$$\varepsilon_s(\omega) = \frac{n_+^2(\omega) + n_-^2(\omega)}{2}, \quad (5)$$

$$\varepsilon_a(\omega) = \frac{n_+^2(\omega) - n_-^2(\omega)}{2}. \quad (6)$$

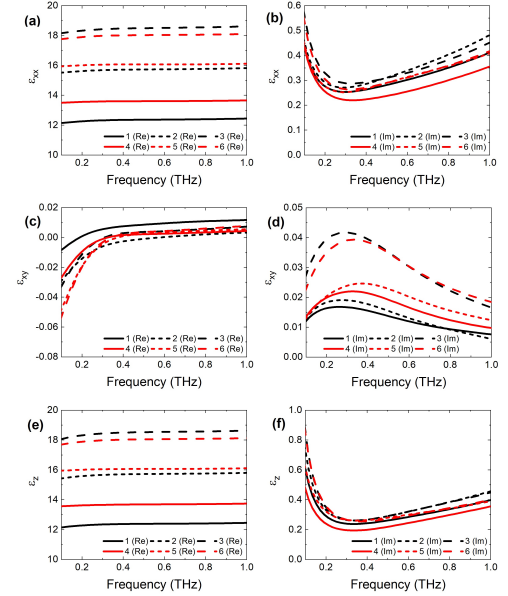


FIG. 5. The permittivity tensor components spectra of 1-mm thick  $\text{BaAl}_x\text{Fe}_{12-x}\text{O}_{19}$ : the real parts of  $\varepsilon_{xx}$  (a),  $\varepsilon_{xy}$  (c) and  $\varepsilon_z$  (e), and the imaginary parts of  $\varepsilon_{xx}$  (b),  $\varepsilon_{xy}$  (d) and  $\varepsilon_z$  (f). Samples are marked according to the Table I.

The refractive indices could be obtained by standard extraction method<sup>20</sup>:

$$n_{\pm}(\omega) = 1 + \frac{c}{\omega d} (\arg(E_{\pm}^{sam}(\omega)) - \arg(E_{\pm}^{ref}(\omega))), \quad (7)$$

where  $E_{\pm}^{sam}(\omega)$  and  $E_{\pm}^{ref}(\omega)$  are the complex electric field spectra of the right and left circularly polarized wave transmitted through the sample and air, correspondingly<sup>23</sup>:

$$E_+(\omega) = \frac{(i+1)E_{+45}(\omega) + (i-1)E_{-45}(\omega)}{2}, \quad (8)$$

$$E_-(\omega) = \frac{(i-1)E_{+45}(\omega) + (i+1)E_{-45}(\omega)}{2}. \quad (9)$$

It should be noted that  $\varepsilon_z$  is the same as  $\varepsilon_s$  for the non-magnetized sample. The  $\varepsilon_z$  spectra were extracted for all samples after oven-enclosing with a temperature above Curie temperature. Extracted dielectric tensor components of each investigated hexaferrite sample are presented in Fig. 5.

As seen from Fig 5 the difference between the  $\varepsilon_{xx}$  and  $\varepsilon_z$  is negligible. The real parts of  $\varepsilon_{xx}$  and  $\varepsilon_z$  exhibit quasi-dispersionless behavior within the considered frequency range

and follow the character of the Faraday rotation spectra. The permittivity component for non-magnetized hexaferrite  $\epsilon_z$  is in good agreement with previously reported results<sup>15</sup>.

Using extracted permittivity tensor components, Faraday rotation can be calculated as<sup>24,25</sup>:

$$\theta_F = \frac{\arg(T_+) - \arg(T_-)}{2}, \quad (10)$$

where  $T_+$  and  $T_-$  are complex transmittances for right-handed circularly polarized (RCP) and left-handed circularly polarized (LCP) waves<sup>24,25</sup>:

$$T_{\pm} = \frac{4(\sqrt{\epsilon_s \mp \epsilon_a})}{1 + \sqrt{\epsilon_s \mp \epsilon_a}} \exp\left(j \frac{\sqrt{\epsilon_s \mp \epsilon_a} + 1}{c} d\right), \quad (11)$$

where  $c$  is the vacuum speed of light. By calculation of Faraday rotation using Eq. 10 and Eq. 11, the excellent agreement with data calculated using Eq. 1 was obtained (see symbols in Fig. 3).

In conclusion, strong non-dispersive Faraday rotation up to 20° in 1-mm thick magnetized aluminum-substituted barium hexaferrite at terahertz frequencies was observed. By controlling the density of hexaferrite sample as well as the concentration of Al dopant it is possible to adjust the Faraday rotation angle and insertion losses. The results give guidance on the choice of the most optimal hexaferrite for utilization as a basis of the self-biased terahertz nonreciprocal isolator.

#### ACKNOWLEDGMENTS

This work was performed using the resources of Tydex LLC.

#### DATA AVAILABILITY

The data that support the findings of this study are available from the corresponding author upon reasonable request.

<sup>1</sup>F. Fan, S. Chen, and S.-J. Chang, "A review of magneto-optical microstructure devices at terahertz frequencies," *IEEE Journal of Selected Topics in Quantum Electronics* **23**, 1–11 (2016).

<sup>2</sup>A. Ishimaru, *Electromagnetic wave propagation, radiation, and scattering: from fundamentals to applications* (John Wiley & Sons, 2017).

<sup>3</sup>M. Tamagnone, C. Moldovan, J.-M. Pouirol, A. B. Kuzmenko, A. M. Ionescu, J. R. Mosig, and J. Perruisseau-Carrier, "Near optimal graphene terahertz non-reciprocal isolator," *Nature communications* **7**, 1–6 (2016).

<sup>4</sup>A. Grebenchukov, S. Azbite, A. Zaitsev, and M. Khodzitsky, "Faraday effect control in graphene-dielectric structure by optical pumping," *Journal of Magnetism and Magnetic Materials* **472**, 25–28 (2019).

<sup>5</sup>Y. Ji, F. Fan, Z. Tan, and S. Chang, "Terahertz nonreciprocal isolator based on magneto-plasmon and destructive interference at room temperature," *Front. Phys.* **8**, 334. doi: 10.3389/fphy (2020).

<sup>6</sup>F. Fan, S.-J. Chang, W.-H. Gu, X.-H. Wang, and A.-Q. Chen, "Magnetically tunable terahertz isolator based on structured semiconductor magneto-plasmonics," *IEEE Photonics Technology Letters* **24**, 2080–2083 (2012).

<sup>7</sup>S. Lin, S. Silva, J. Zhou, and D. Talbayev, "A one-way mirror: High-performance terahertz optical isolator based on magnetoplasmonics," *Advanced Optical Materials* **6**, 1800572 (2018).

<sup>8</sup>J. Ding, W. Jin, Q. Chen, C. Hou, Y. Yu, L. Su, C. Li, F. Zeng, and A. Wu, "Optical properties, magneto-optical properties and terahertz time-domain spectrum of tb 3 sc 2 al 3 o 12 crystals grown by optical floating zone methods," *Optical Materials Express* **8**, 2880–2886 (2018).

<sup>9</sup>Y.-L. Li, T.-F. Li, Q.-Y. Wen, F. Fan, Q.-H. Yang, and S.-J. Chang, "Terahertz magneto-optical effect of wafer-scale la: yttrium iron garnet single-crystal film with low loss and high permittivity," *Optics Express* **28**, 21062–21071 (2020).

<sup>10</sup>M. Shalaby, M. Peccianti, Y. Ozturk, and R. Morandotti, "A magnetic non-reciprocal isolator for broadband terahertz operation," *Nature communications* **4**, 1–7 (2013).

<sup>11</sup>B. Yang, R. J. Wylde, D. H. Martin, P. Goy, R. S. Donnan, and S. Caeroopen, "Determination of the gyrotropic characteristics of hexaferrite ceramics from 75 to 600 ghz," *IEEE transactions on microwave theory and techniques* **58**, 3587–3597 (2010).

<sup>12</sup>C. Caloz and Z.-L. Deck-Léger, "Spacetime metamaterials—part ii: Theory and applications," *IEEE Transactions on Antennas and Propagation* **68**, 1583–1598 (2019).

<sup>13</sup>D. L. Sounas and A. Alu, "Nonreciprocity based on nonlinear resonances," *IEEE Antennas and Wireless Propagation Letters* **17**, 1958–1962 (2018).

<sup>14</sup>I. B. Vendik, O. G. Vendik, M. A. Odit, D. V. Kholodnyak, S. P. Zubko, M. F. Sitnikova, P. A. Turalchuk, K. N. Zemlyakov, I. V. Munina, D. S. Kozlov, *et al.*, "Tunable metamaterials for controlling thz radiation," *IEEE Transactions on Terahertz Science and Technology* **2**, 538–549 (2012).

<sup>15</sup>T. Horák, G. Ducoumau, M. Mičica, K. Postava, J. B. Youssef, J.-F. Lampin, and M. Vanwolleghem, "Free-space characterization of magneto-optical hexaferrites in the submillimeter-wave range," *IEEE Transactions on Terahertz Science and Technology* **7**, 563–571 (2017).

<sup>16</sup>V. G. Harris, A. Geiler, Y. Chen, S. D. Yoon, M. Wu, A. Yang, Z. Chen, P. He, P. V. Parimi, X. Zuo, *et al.*, "Recent advances in processing and applications of microwave ferrites," *Journal of Magnetism and Magnetic Materials* **321**, 2035–2047 (2009).

<sup>17</sup>B. Yang and R. S. Donnan, "Enhanced rapid and accurate sub-thz magneto-optical characterization of hexaferrite ceramics," *Journal of magnetism and magnetic materials* **323**, 1992–1997 (2011).

<sup>18</sup>M. Born and E. Wolf, *Principles of optics: electromagnetic theory of propagation, interference and diffraction of light* (Elsevier, 2013).

<sup>19</sup>A. V. Kuzikova, A. V. Vozianova, and M. K. Khodzitsky, "Extraction the diagonal and off-diagonal components of permittivity tensor using terahertz time-domain polarimetry," in *Fourth International Conference on Terahertz and Microwave Radiation: Generation, Detection, and Applications*, Vol. 11582 (International Society for Optics and Photonics, 2020) p. 115821O.

<sup>20</sup>M. Naftaly, *Terahertz metrology* (Artech House, 2015).

<sup>21</sup>V. N. Dhage, M. Mane, A. Keche, C. Birajdar, and K. Jadhav, "Structural and magnetic behaviour of aluminium doped barium hexaferrite nanoparticles synthesized by solution combustion technique," *Physica B: Condensed Matter* **406**, 789–793 (2011).

<sup>22</sup>B. Yang, X. Wang, Y. Zhang, and R. S. Donnan, "Experimental characterization of hexaferrite ceramics from 100 ghz to 1 thz using vector network analysis and terahertz-time domain spectroscopy," *Journal of Applied Physics* **109**, 033509 (2011).

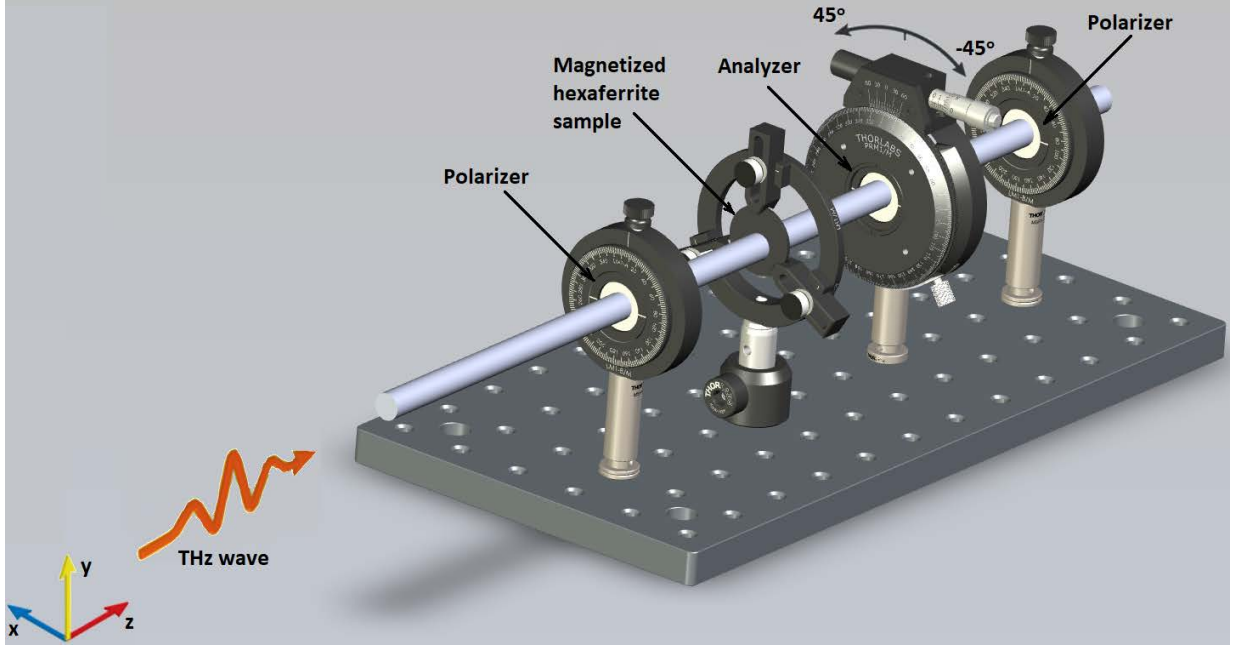
<sup>23</sup>F. Fan, S. Chen, W. Lin, Y.-P. Miao, S.-J. Chang, B. Liu, X.-H. Wang, and L. Lin, "Magnetically tunable terahertz magnetoplasmons in ferrofluid-filled photonic crystals," *Applied Physics Letters* **103**, 161115 (2013).

<sup>24</sup>E. Palik and J. Furdyna, "Infrared and microwave magnetoplasma effects in semiconductors," *Reports on Progress in Physics* **33**, 1193 (1970).

<sup>25</sup>O. Morikawa, A. Quema, S. Nashima, H. Sumikura, T. Nagashima, and M. Hangyo, "Faraday ellipticity and faraday rotation of a doped-silicon wafer studied by terahertz time-domain spectroscopy," *Journal of applied physics* **100**, 033105 (2006).

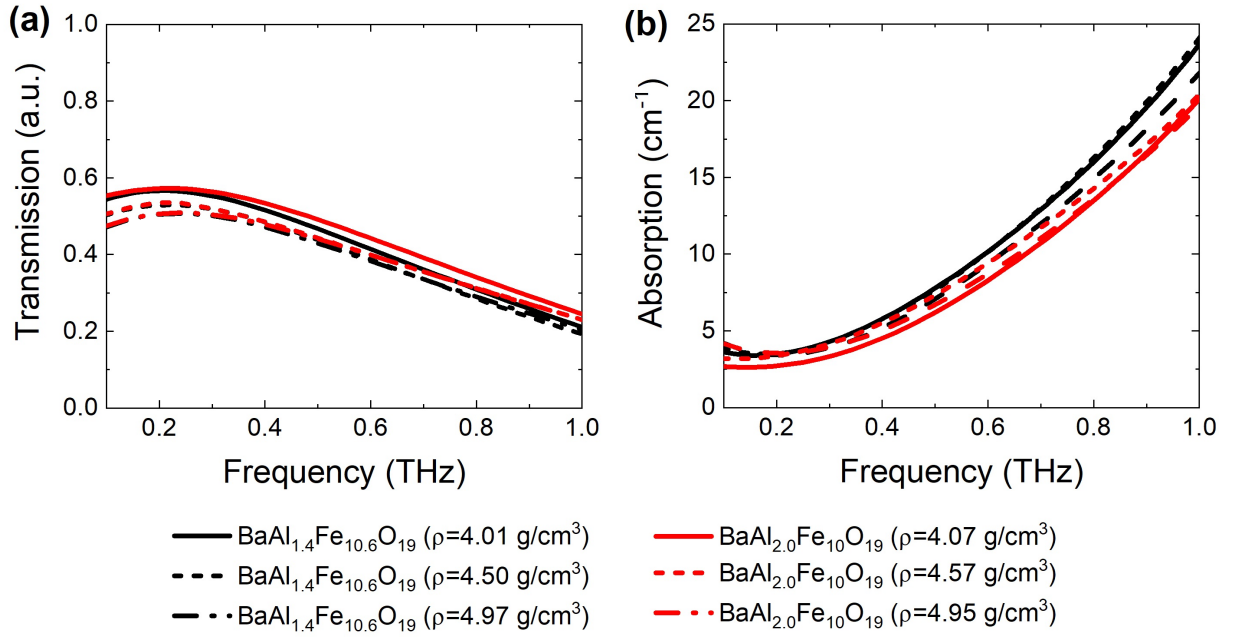
This is the author's peer reviewed, accepted manuscript. However, the online version of record will be different from this version once it has been copyedited and typeset.

PLEASE CITE THIS ARTICLE AS DOI: 10.1063/1.50048604

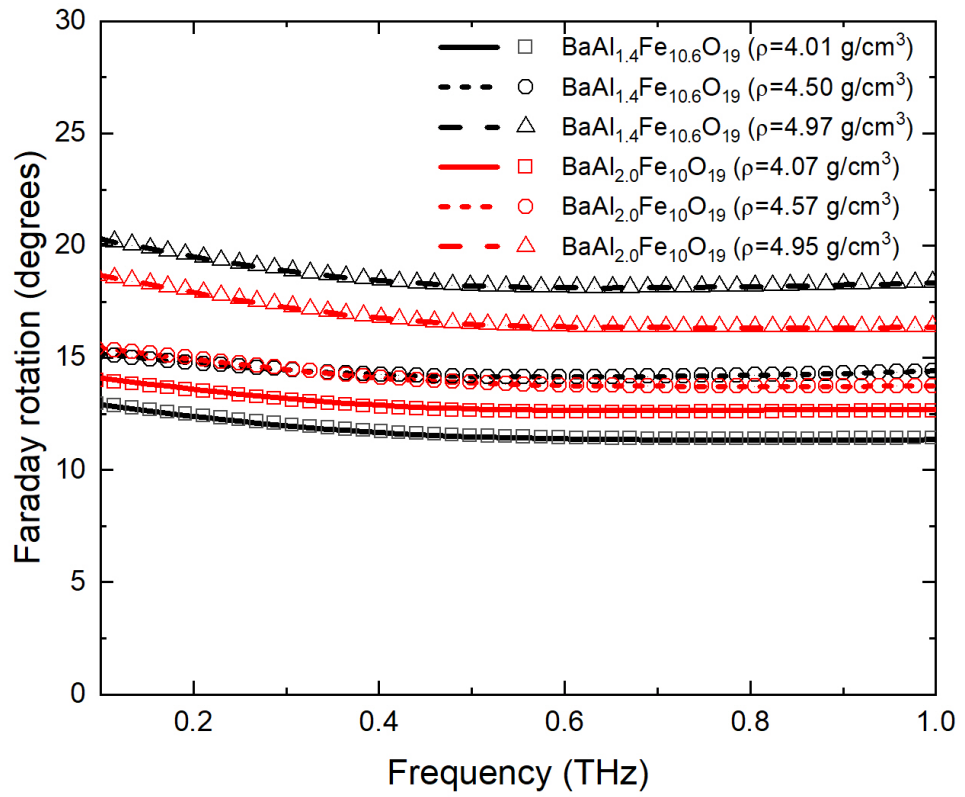


This is the author's peer reviewed, accepted manuscript. However, the online version of record will be different from this version once it has been copyedited and typeset.

PLEASE CITE THIS ARTICLE AS DOI: 10.1063/5.0048604

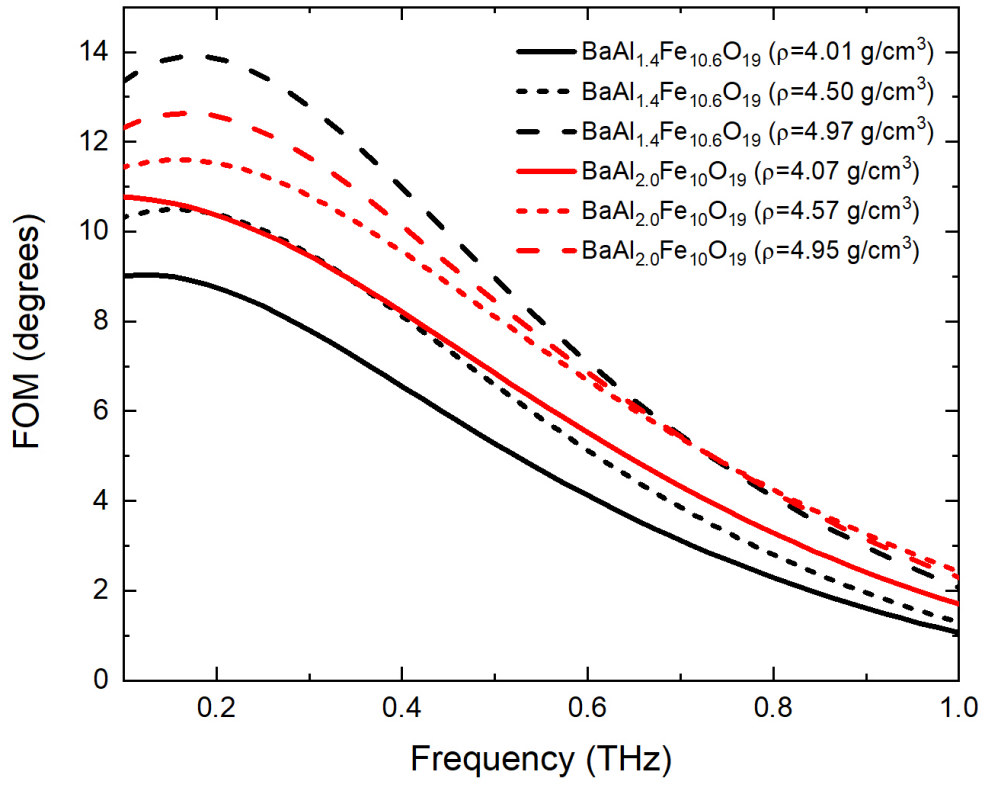


This is the author's peer reviewed, accepted manuscript. However, the online version of record will be different from this version once it has been copyedited and typeset.  
 PLEASE CITE THIS ARTICLE AS DOI: 10.1063/1.50048604



This is the author's peer reviewed, accepted manuscript. However, the online version of record will be different from this version once it has been copyedited and typeset.

PLEASE CITE THIS ARTICLE AS DOI: 10.1063/5.0048604



This is the author's peer reviewed, accepted manuscript. However, the online version of record will be different from this version once it has been copyedited and typeset.

PLEASE CITE THIS ARTICLE AS DOI: 10.1063/5.0048604

